J. Fluid Mech. (1974), *vol.* 66, *part* 4, *pp.* 625–640
Printed in Great Britain

Wave breaking in the presence of wind drift and swell

By O. M. PHILLIPS AND M. L. BANNER†
Department of Earth and Planetary Sciences, The Johns Hopkins University, Baltimore, Maryland 21218

(Received 6 March 1974)

Wind, blowing over a water surface, induces a thin layer of high vorticity in which the wind stress is supported by molecular viscosity; the magnitude of the surface drift, the velocity difference across the layer, being of the order of 3 % of the wind speed. When long waves move across the surface, there is a nonlinear augmentation of the surface drift near the long-wave crests, so that short waves, superimposed on the longer ones, experience an augmented drift in these regions. This is shown to *reduce* the maximum amplitude that the short waves can attain when they are at the point of incipient breaking.

Theoretical estimates of the reduction are compared with measurements in wind–wave tanks by the authors and by Mitsuyasu (1966) in which long mechanically generated waves are superimposed on short wind-generated waves. The reductions measured in the energy density of the short waves by increasing the slope of the longer ones at constant wind speed are generally consistent with the predictions of the theory in a variety of cases.

1. Introduction

At sea, when long waves sweep through a field of shorter wind-generated waves, variations result in the energy density of the short waves with respect to the phase of the longer ones. Longuet-Higgins & Stewart (1960) showed that the amplitude of a short irrotational wave of small slope is greatest at the long-wave crest and least at the trough, partly as a result of the geometrical convergence at the crest and partly as a result of the working by radiation stresses. On this basis alone, it might be conjectured that the short waves would break preferentially near the long-wave crests, so that the mean amplitude of the short-wave train would be limited by the breaking in the vicinity of the long-wave crests.

In an earlier paper by us (Banner & Phillips 1974) it was shown that the presence of a thin wind drift layer with high vorticity near the surface causes breaking to occur at a wave amplitude substantially less than that associated with the Stokes limiting form with a sharp crest. A characteristic of breaking waves is the occurrence of a region at the surface and near the wave crest where the fluid elements are moving faster than the wave profile: they tumble forwards

† Present address: School of Mathematics, The University of New South Wales, Kensington, New South Wales, Australia 2033.

down the front face of the wave. When the wave is at the point of incipient breaking, the surface velocity at the wave crest must approach the phase velocity of the wave; relative to the wave profile, the fluid elements must come to rest at the wave crest. In a purely irrotational motion, this coincides with the Stokes limit, but when there is a surface wind drift in the same direction as the wave propagation, the speed of the fluid elements at the surface is everywhere less relative to the profile (by the amount of the wind drift) than it is in a purely irrotational wave. Accordingly, the maximum vertical distance that the surface fluid elements can rise before coming to rest is correspondingly reduced. If the effects of molecular viscosity are neglected, the elevation of the crests in a single wave train at the point of incipient breaking was shown by Banner & Phillips (1974) to be

$$\zeta_{\max} = (C^2/2g)\,(1-\gamma)^2, \tag{1.1}$$

where $\gamma = q_0/C$, the ratio of the surface drift at the mean water level (where $\zeta = 0$) to the phase speed of the wave.

The magnitude of the surface drift, the velocity of the fluid elements at the surface relative to those immediately below the vortical layer and in the essentially irrotational region,† varies with respect to the phase of the wave. Near the crest of a long wave that may itself not be near the condition (1.1) for incipient breaking, the convergence of the layer leads to its thickening and an augmentation of the forward drift at the surface. A short wave riding over the longer wave will experience an increased drift near the long-wave crest, while at the same time its phase speed is reduced by the convergence. On both accounts, γ is greater here than elsewhere, and the short wave will attain a condition of incipient breaking at a *smaller* amplitude when it is near the crest of a long wave than elsewhere.

The exploration of these processes, both theoretically and experimentally, is the subject of the present paper. In the laboratory, it has already been observed by Mitsuyasu (1966) and by Bole & Hsu (1967) that when mechanically generated long waves are superimposed on short wind-generated waves, there is a substantial reduction in the average spectral density of the shorter waves, an effect that increases markedly with the slope of the longer wave. We have observed the same phenomenon – some of our results are described later – but we are not aware of any serious attempt to account for it quantitatively. It has, of course, profound consequences on the small scale structure of ocean waves since it provides a mechanism for modification of the small structure that is much more immediate and direct than those involved either in the second-order energy exchanges associated with radiation stress effects or in the third-order resonant interactions.

2. The surface drift

When the wind blows over the ocean surface, a tangential stress is communicated to the water and, in the absence of wave breaking, the stress immediately below the surface must be supported by molecular viscosity until the depth is

† In which itself there is a mean Stokes drift.

sufficient for the turbulent Reynolds stresses to dominate. This viscous sublayer will, to be sure, be disrupted from time to time by wave breaking but only to be re-established behind the breaking region. Over most of the surface, even if there is intermittent breaking, a thin layer of relatively high vorticity will separate the surface from the more turbulent fluid below, where the mean velocity gradient and mean vorticity are very much less.

Consider, then, the behaviour of a thin sheet of vorticity $\boldsymbol{\omega}$ parallel to the surface that is strained and convected by the underlying larger scale velocity field $\mathbf{U}(x, y, t)$. In the layer, the velocity field $\mathbf{u}$ varies rapidly and approaches $\mathbf{U}$ below: the vorticity

$$\boldsymbol{\omega} \simeq (-\partial v/\partial z, \partial u/\partial z, 0), \tag{2.1}$$

where the z axis is taken normal to the surface and x and y parallel to it. The vorticity balance is

$$\frac{\partial \omega_i}{\partial t} + \frac{\partial}{\partial x_j}(u_j \omega_i) = \frac{\partial}{\partial x_j}(\omega_j u_i) + \nu \frac{\partial^2}{\partial x_j^2} \omega_i, \tag{2.2}$$

and inside the layer, this reduces to

$$\frac{\partial}{\partial t}\frac{\partial u}{\partial z} + \frac{\partial}{\partial x}\left(u\frac{\partial u}{\partial z}\right) + \frac{\partial}{\partial z}\left(w\frac{\partial u}{\partial z}\right) = \frac{\partial}{\partial x}\left(-v\frac{\partial v}{\partial z}\right) + \nu\frac{\partial^3 u}{\partial z^3},$$

for the 2- or y-component, in which the horizontal diffusion of vorticity by molecular viscosity is neglected on account of the very large horizontal scale compared with the vertical one. When it is integrated across the layer, this equation reduces to

$$\frac{\partial}{\partial t}\Delta u + \frac{1}{2}\frac{\partial}{\partial x}\Delta(u^2 + v^2) = \nu\Delta\frac{\partial^2 u}{\partial z^2}, \tag{2.3}$$

where the symbol Δ specifies the difference across the layer. A similar equation can be found involving Δv, so that in general

$$\frac{\partial}{\partial t}\Delta\mathbf{u} + \tfrac{1}{2}\nabla\Delta(u^2 + v^2) = \nu\Delta\frac{\partial^2 u}{\partial z^2}. \tag{2.4}$$

If $\mathbf{q} = \Delta\mathbf{u}$ represents the local drift at the surface, the velocity of the fluid elements at the surface relative to those below the vortical layer, then, at the surface, $\mathbf{u} = \mathbf{U} + \mathbf{q}$ and beneath the layer $\mathbf{u} = \mathbf{U}$, so that

$$\partial\mathbf{q}/\partial t + \nabla\{\mathbf{U}.\mathbf{q} + \tfrac{1}{2}q^2\} = \Delta(\partial\boldsymbol{\tau}/\partial z), \tag{2.5}$$

where $\boldsymbol{\tau} = \nu\,\partial\mathbf{u}/\partial z$ is the tangential component of the molecular viscous stress acting across the layer, divided by the water density, and $\mathbf{U}$ is the underlying (substantially irrotational) velocity field.

The last term describes the acceleration of the surface relative to the underlying fluid as a result of the difference in tangential stress gradient, and it is rather difficult to estimate with any precision its order of magnitude relative to the convective term. Certainly it is centrally important in the re-establishment of the vortical layer after it has been disrupted by wave breaking, but its influence

might be expected to diminish thereafter. In a horizontally statistically stationary and steady motion, its mean value vanishes, the viscous stress being in essence constant across the sublayer. *Variations* in tangential wind stress, perhaps induced by the wave displacement, will produce variations in τ, say $\delta\tau$, so that the last term may be of order $\delta\tau/d$, where d is the sublayer thickness. In a well-developed sublayer, in the absence of wave distortion, the velocity difference q is of the order $10\,w_*$, where $w_* = (\tau/\rho_w)^{\frac{1}{2}}$ is the friction velocity in the water. In a wave of radian frequency σ, the terms on the left of (2.5) are of the order $10\sigma w_*$, so that the viscous term can be neglected if

$$\delta\tau/d \ll 10\sigma w_*$$

or

$$\delta\tau/\tau \ll 10\sigma d/w_*.$$

If this is so, (2.5) can be approximated by

$$\partial\mathbf{q}/\partial t + \nabla\{\mathbf{U}.\mathbf{q} + \tfrac{1}{2}q^2\} = 0, \tag{2.6}$$

which specifies $\mathbf{q}(x, y, t)$ in terms of $\mathbf{U}$ or, equivalently, the distribution $\mathbf{U}(x, y, t)$ required to generate a given $\mathbf{q}$ from a prescribed initial state. Note that only the component of $\mathbf{U}$ in the direction of $\mathbf{q}$ is involved; the perpendicular component stretches the vortex lines but the thickness of the layer is reduced proportionately, so that the relative drift $\mathbf{q}$ is unaffected. Note also that the neglect of viscous effects would be expected to underestimate the augmentation of the surface drift of mean wave crests, an increased tangential wind stress near the crests providing an additional acceleration in the drift layer.

For a single wave train with phase speed C the distribution of surface drift can be found immediately. The motion is steady in a frame of reference moving with speed C, so that

$$Uq + \tfrac{1}{2}q^2 = \text{constant} = -Cq_0 + \tfrac{1}{2}q_0^2, \tag{2.7}$$

where q_0 is the surface drift at the point of the wave profile where the surface displacement $\zeta = 0$; the (irrotational) velocity below the surface layer at this point is $-C$ parallel to the surface as shown by Levi Civita (see Lamb 1953, p. 420). This equation leads to the condition for incipient breaking of a single wave train as given in a previous paper (Banner & Phillips 1974). At the wave crest, $U = -C + u_0$, where u_0 is the orbital speed of the wave at the crest, so that the speed at the surface is $U + q = -C + u_0 + q$, which vanishes when

$$(C - u_0)^2 = q_0(2C - q_0). \tag{2.8}$$

If $u(s)$ represents the tangential component of the orbital velocity in the wave, a periodic function of position along the profile, then, in a wave of small slope,

$$U \simeq -C + u(s)$$

and the distribution of surface drift q in the wave is given by the solution to the quadratic (2.7):

$$q = (C - u) - \{(C - u)^2 - q_0(2C - q_0)\}^{\frac{1}{2}}, \tag{2.9}$$

the negative sign being chosen since $q \to q_0$ as $u \to 0$. Since the slope is small, $u = u_0 \cos\theta$, where θ is the phase, $\theta = 0$ being at the crest. Some distributions of

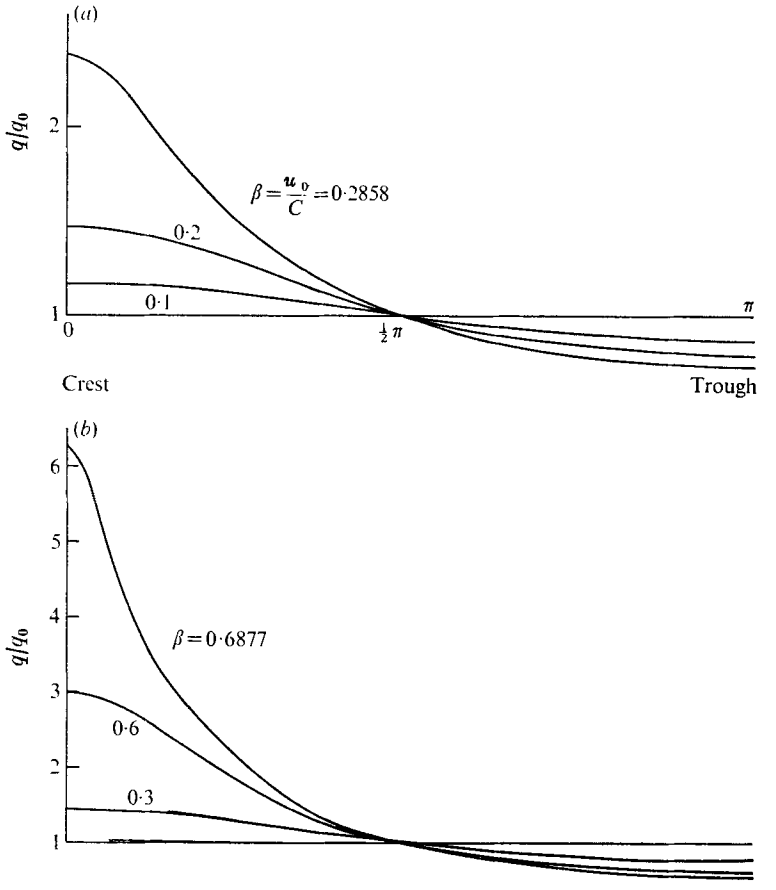

FIGURE 1. The distribution of surface drift with respect to phase of a wave. (*a*) The distribution when the drift q_0 at the mean water level is 0·3 times the phase speed C for values of the ratio of maximum orbital velocity to phase speed (wave slope, approximately) ranging up to 0·2858, the point of incipient breaking in this case. In (*b*) the ratio q_0/C is 0·05 and $u_0/C = 0{\cdot}6788$ at the point of incipient breaking, when the surface drift at the crest is augmented by a factor greater than six.

q/q_0 are shown in figure 1. Note that, when the waves are not near the condition for incipient breaking, the surface drift varies approximately as $\cos\theta$, but, as this limit is approached, the drift near the wave crests increases rapidly. The amplification of the drift current at crests by waves of a given slope is illustrated as a function of C/q_0 in figure 2. The curves terminate at the point of incipient breaking and, for waves of a given slope that are near this limit, the amplification rate varies rapidly with C/q_0. When C/q_0 is much larger than the critical value for a given slope, however, the variation is clearly much slower.

If, now, a short wave is riding over a long wave, and being overtaken by it, the surface drift velocities are not simply additive because of the nonlinearity of (2.6). However, at a given phase of the long wave, the short wave experiences the augmented drift q (at the point where the *short*-wave displacement and the associated surface-layer strain are zero), which is in turn further increased by the

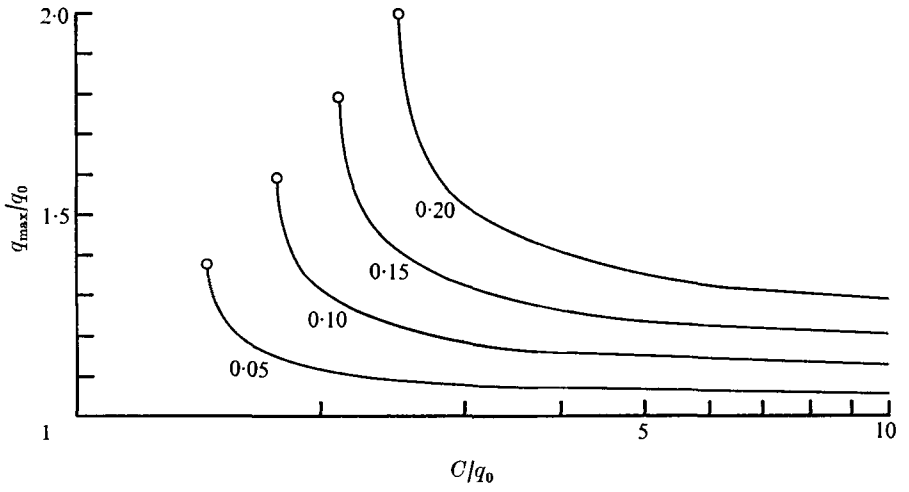

FIGURE 2. The maximum augmentation of drift (at the wave crest) for waves of a given slope as a function of C/q_0. Each curve terminates at the point of incipient breaking.

convergence of the short wave. If the short wave is propagating with local speed c relative to the velocity below the vortical layer, and u_0 is the maximum orbital velocity at the short wave, then the condition for incipient breaking of the short wave at this point on the long wave is

$$(c-u_0)^2 = q(2c-q), \tag{2.10}$$

where q, the local drift as augmented by the long wave, is given by (2.9). An infinitesimal wave of even vanishingly small amplitude ($u_0 \to 0$) will break when $q = c$, when the drift induced by the long wave attains the local phase speed of the *short* wave. This occurs in a long wave of small slope when

$$c = (C - \mathscr{U}_0 \cos\theta) - \{(C-\mathscr{U}_0\cos\theta)^2 - q_0(2C-q_0)\}^{\frac{1}{2}},$$

where $\mathscr{U}_0$ is the maximum orbital velocity of the long wave or, for given values of the drift q_0 at the reference point on the long wave, c and C, when

$$\frac{\mathscr{U}_0\cos\theta}{C} = 1 - \frac{c}{2C} - \frac{C}{c}\frac{q_0}{C}\left(1-\frac{q_0}{2C}\right). \tag{2.11}$$

It follows that short wavelets of even infinitesimal amplitude cannot move past a long-wave crest ($\theta = 0$) unless

$$\mathscr{U}_0/C < 1 - \tfrac{1}{2}\alpha - \alpha^{-1}\gamma(1-\tfrac{1}{2}\gamma), \tag{2.12}$$

where $\gamma = q_0/C$ and $\alpha = c/C$, the ratio of the short-wave phase speed at the crest of the long wave to the phase speed of the long wave itself. Note that, when $\alpha = \gamma$, the short waves are at the point of incipient breaking even when $u_0 = 0$, so that $\alpha > \gamma > 0$. Moreover, $\alpha^2 = (c/C)^2 \simeq \lambda/\Lambda$, the ratio of the two wavelengths for gravity waves, which is necessarily small compared with unity. The condition (2.12) is illustrated in figure 3. For given values of the wind drift, i.e. of q_0/C and of the ratio α of short-to-long phase speeds, the curves specify the maximum

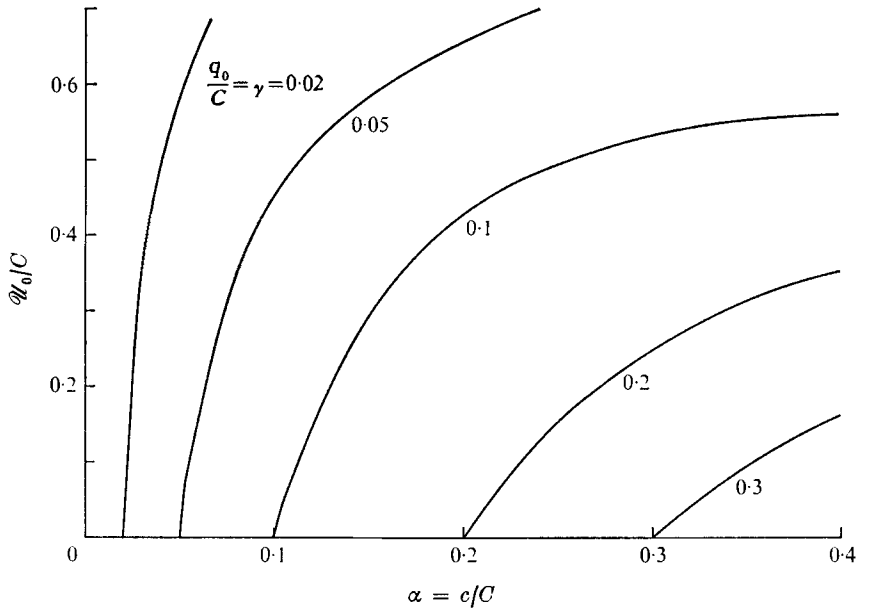

FIGURE 3. The conditions under which short waves cannot propagate through a long-wave crest. For given ratios of short-to-long wave phase speeds α and of the reference drift q_0 to a long-wave speed (γ), the curves specify the maximum ratio of orbital speed $\mathscr{U}_0$ of the long wave to phase speed C that allows the short waves to pass beyond the long-wave crest.

orbital speeds $\mathscr{U}_0$ at the long-wave crest that can allow infinitesimal wavelets to pass through the crest. In the ocean, with short waves riding over long swell, the appropriate values of γ are small (of order 0·05), whereas in the laboratory, with relatively short mechanically generated waves interacting with wind waves, substantially higher values will be found.

3. Kinematics of the short waves

In the previous section, c specifies the *local* phase speed of the short-wave train relative to the fluid underlying the wind drift layer. As a result of the straining associated with long waves, the short wavelength and so c varies somewhat with respect to the phase of the long wave. Previous analyses by Longuet-Higgins & Stewart (1960) and Phillips (1968, p. 61) have used small perturbation expansions; more general results can be derived simply. In a frame of reference moving with speed C, the pattern of short waves is independent of time, so that from the kinematical conservation equation, the number of short-wave crests passing a fixed point per unit time is constant over the long-wave profile. The propagation of short waves is influenced by the combined orbital and streaming motion associated with the long wave (which is, in essence, constant over a depth of the order of the wavelength of the short waves) but very little by the surface drift provided it is confined to a depth much smaller than the short wavelength. In the ocean, we shall be concerned with short gravity wavelengths of the order of

10 or 20 cm at least and layer depths that are fractions of a centimetre; in these circumstances the influence of q on c might be neglected safely. It is not, however, certain; the continual breaking of short waves injects momentum that may extend downwards to possibly one-tenth of the wavelength of the short waves and the rapidity with which this is smoothed out depends presumably on the ambient turbulence level in the water below the surface. In the laboratory, the inequality is satisfied less well and some account should properly be taken of the changes that occur in the short-wave speed as a result of the surface drift. Nevertheless, in the following analysis, it will be neglected.

As the short-wave pattern is swept over the long-wave crests, the apparent gravitational acceleration is less than g by the amount of the vertical acceleration that a wave packet experiences. Longuet-Higgins & Stewart (1960) point out that the apparent acceleration is $g' = g + \ddot{Z}$, where $z = Z(x,t)$ is the profile of the long wave. If the long wave is of small slope,

$$g' = g(1 - 2\pi Z/\Lambda) = g'(s), \quad \text{say}, \tag{3.1}$$

where Λ is the long wavelength. The dispersion relation for short gravity waves is then $\sigma = (g'k)^{\frac{1}{2}}$ and the conservation of short waves in a frame of reference moving with the long waves is

$$\sigma + k(\mathscr{U} - C) = \text{constant},$$

where the second term represents the convection of waves by the combined orbital speed $\mathscr{U}$ of the long waves and the mean streaming associated with our translation of the frame of reference. Thus

$$(g'k)^{\frac{1}{2}} + k(\mathscr{U} - C) = (gk_0)^{\frac{1}{2}} - k_0 C = -n_0, \quad \text{say}, \tag{3.2}$$

where k_0 is the local wavenumber when $Z = 0$; at this point $g' = g$ and the fluid speed (below the surface layer) is equal precisely to $-C$.

Equation (3.2) is a quadratic in $k^{-\frac{1}{2}}$ or equivalently in $c = (g'/k)^{\frac{1}{2}}$:

$$(n_0/g')\, c^2 + c - (C - \mathscr{U}) = 0. \tag{3.3}$$

If the long wave has small slope, $g' = g(1 - \beta\cos\theta)$, where β is the long-wave slope and $\mathscr{U} = \mathscr{U}_0 \cos\theta$. From (3.2),

$$n_0/g = (C - c_0)/c_0^2.$$

The substitution of these expressions into (3.3) gives

$$\frac{1-\alpha}{\alpha^2(1-\beta\cos\theta)}\left(\frac{c}{C}\right)^2 + \frac{c}{C} - (1 - \beta\cos\theta) = 0,$$

where $\alpha = c_0/C$. Since $c/C \to \alpha$ when $\theta = \frac{1}{2}\pi$, the appropriate root is

$$c/C = \alpha(1 - \beta\cos\theta). \tag{3.4}$$

Note that the phase speed c of the short wave is reduced as the crest is approached while the ambient drift q increases; *a fortiori* the ratio c/q decreases. If $c/q = 1$ at some point on the long wave, even infinitesimal amplitude short waves cannot propagate as has already been pointed out: the short waves dissipate on the

forward face in a series of small scale breaking crests that disappear when the long-wave crest is approached.

If the phase speed of the short wave at a long-wave crest is greater than the local drift q, waves of non-zero amplitude can move past this point without breaking. What is the maximum amplitude that these wavelets can have when they are at the point of incipient breaking at the long-wave crest? From (1.1)

$$\zeta_{\max} = (2g')^{-1}(c_c - q_{\max})^2, \tag{3.5}$$

where $q_{\max}$, the maximum value of the drift augmented by the long wave, is given from (2.9),

$$q_{\max} = (C - u_0) - \{(C-u_0)^2 - q_0(2C - q_0)\}^{\frac{1}{2}}, \tag{3.6}$$

and the short-wave phase speed c_c at the crest is given by (3.4) with $\theta = 0$.

In (3.6) C represents the phase speed of the long wave and u_0 its maximum orbital velocity. The ratio r of the maximum wavelet amplitude to what it would be in the absence of the long wave is, from (1.1) and (3.5),

$$r = \left(\frac{g}{g'}\right)\frac{(c_c - q_{\max})^2}{(c_0 - q_0)^2}, \tag{3.7}$$

which is an algebraic function of the three parameters $\alpha = c_0/C$, $\beta = u_0/C$ and $\gamma = q_0/C$ that can be found immediately from (3.4) and (3.6).

4. The suppression of short wind waves by longer ones

The suppression of short wind-generated waves by a train of longer, mechanically generated waves was apparently observed first by Mitsuyasu (1966) in a laboratory study. As the slope of the long waves increased, the total energy density and the spectral density of the short waves decreased progressively. Mitsuyasu's experimental conditions were unfortunately not very well defined – the wind field was far from homogeneous over the surface and the surface drift was not measured – but the phenomenon was striking. For example, with a slope (ak) of the mechanically generated waves of approximately 0·2, Mitsuyasu reported a reduction in the mean-square amplitude of the short waves to less than 40 % of the value in the absence of long waves, all other conditions being the same.

More carefully controlled experiments were conducted in our wind–wave tank and these are described in detail by Banner (1973). Briefly, the tank is 48 ft (14·6 m) long, 42 in. (1·06 m) wide and 2 ft (61 cm) deep, and is fitted with a beach and mechanical wave generator at one end and an absorbent beach at the other. It is coupled with a wind tunnel which has a filtered air intake, an axial blower, an expansion section, a right-angle bend with turning vanes and screens, a settling chamber, an 8:1 vertical contraction and a transition section joining the tunnel to the air channel, 6 in. (15 cm) deep above the water surface of the wave tank. To accelerate the development of a fully developed turbulent channel flow in the working section, three rows of coiled springs were attached to the floor and the roof of the entrance of the transition section, which extended a total of 72 channel heights to the test section.

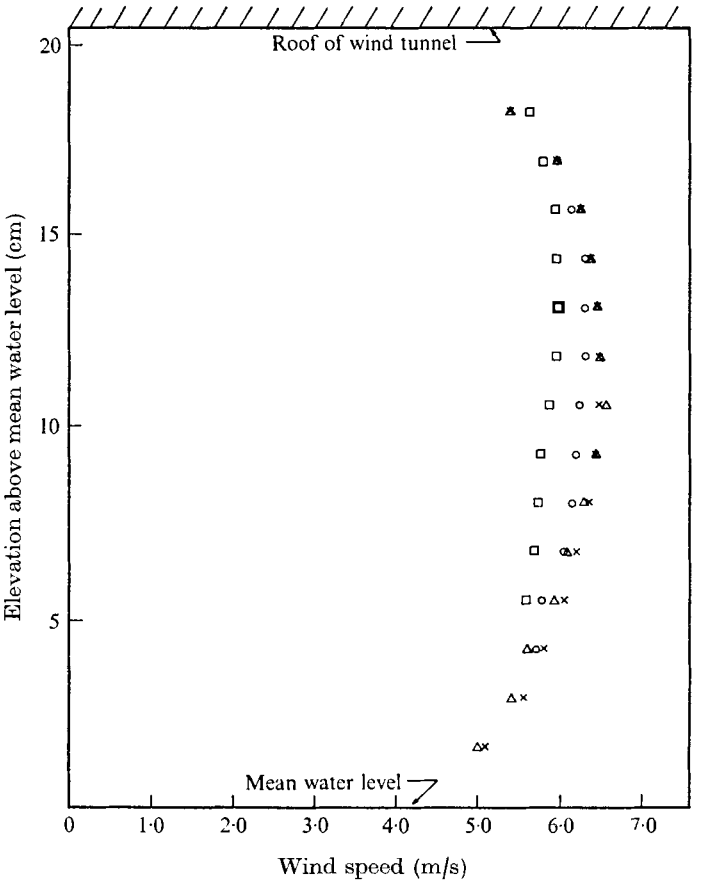

FIGURE 4. The mean velocity profile in the wind–wave tank. Root-mean-square wave amplitudes: ×, 0·3 cm; △, 0·5 cm; ○, 1·5 cm; □, 2·7 cm.

The mean velocity profiles in the air flow, measured with a Pitot-static tube 7·77 m downwind of the wave generator at the fan speed used in our main series of experiments, are shown in figure 4 for various amplitudes of the mechanically generated waves. Under extreme conditions, with a relatively large amplitude breaking wave, the centre-line velocity decreased some 10 % over the value without mechanically generated waves, but the variation over the range discussed here was substantially less. The variation in surface stress over this range was about 5 %. The surface drift was measured by means of computer card punch-outs which were dropped on the water and floated horizontally at the surface. Their downwind motion was timed repeatedly over an 8 ft section of the tank at various wind speeds. Some wind-generated waves were present and allowance was made for the associated Stokes drift, a relatively small correction. On occasion, small scale breaking was observed to carry the punch-outs along with the crest for an interval; these measurements were discarded. The results are shown in figure 5. It is evident that the surface wind drift was a little more than 3 % of the centre-line wind speed, or about $0{\cdot}55\,u_*$. Measurements by Wu (1968)

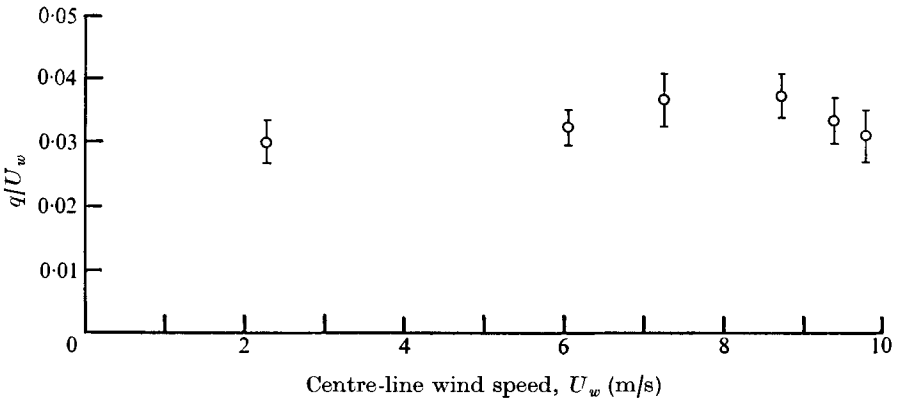

FIGURE 5. The surface drift q as a fraction of the centre-line wind speed U_w in the wind–wave tank, measured by the drift of computer card punch-outs.

in a different wind–wave tank gave surface drifts a little larger than this, approximately 4% of the centre-line velocity, but in view of the variability inherent in each trial and the rather different geometries of the wind–wave tanks, the differences are probably not significant.

At the wind speed used in our main sequence of experiments, 6·06 m/s, the mean drift was 18 ± 2 cm/s. The waves were measured at three different fetches, 4·27 m, 7·32 m and 10·36 m from the wave maker at the upwind end of the tank, making use of impedance probes 0·81 mm in diameter. These were calibrated statically and dynamically. A very slight curvature in the static calibration was corrected in the numerical data processing, and the frequency response was found to be flat to at least 5 Hz. The wave probe outputs were fed into differential analysers where the probe d.c. offset was nulled out, then amplified further and filtered by 100 Hz low-pass Butterworth filters to remove electronic noise. The signals were recorded and digitized by means of a modular analog-to-digital converter. Spectra were calculated using fast Fourier transform methods from data subsets of each run, and these were averaged to provide smoothed spectra. More complete details are given by Banner (1973).

The first set of wave probe measurements and surface photographs was taken at the three fetches under the influence of the wind alone. In the second series of measurements, a mechanically generated wave was superimposed with a frequency (1·7 Hz) lower than those excited by the wind, and a slope of approximately 0·03. The appearance of the water surface was not changed greatly, with sporadic small scale breaking continuing, but when the superimposed wave slope was increased to 0·06, it was evident even by eye that the shorter waves, generated directly by the wind, were much less pronounced. Wave breaking was still sporadic, but limited to the vicinity of the long-wave crests. With a long-wave slope of 0·175, the shorter wave scales present in the original wind-generated waves were not discernible at all: the train of long waves, rather unsteady, was accompanied by patches of parasitic capillaries and freely travelling capillaries, generated by intermittent breaking and irregularities in the wall of the tank.

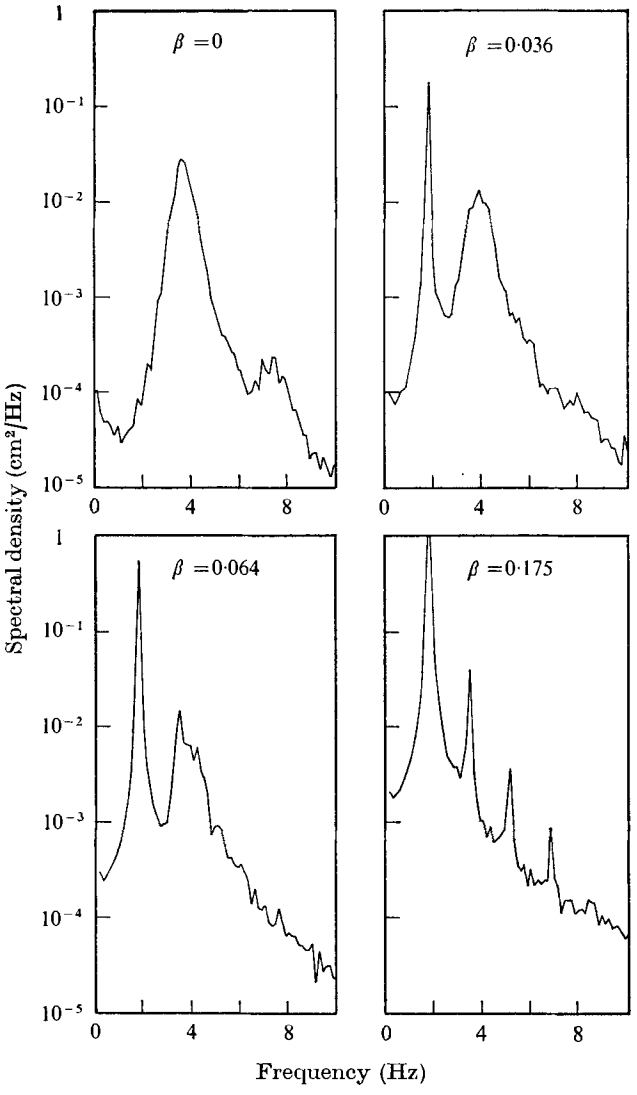

FIGURE 6. A series of wave spectra at constant fetch and wind speed but with increasing slope β of a mechanically generated longer wave. Note that the spectral density decreases with increasing β until, when $\beta = 0{\cdot}175$, only the mechanically generated wave and its harmonics are evident.

These visual observations were consistent with the frequency spectra obtained. A set of spectra measured at the second fetch is shown in figure 6; those at the longest fetch are very similar. At the shortest fetch (4·27 m), the wind-generated wave field was less well developed, being broader and lacking the narrow spectral peak, but in all cases the qualitative response to the superimposed lower frequency wave was similar. The low frequency wave was, in essence, at a single frequency (the shape of the spike reflecting the shape of the numerical filter) and, as its slope increased, the spectral density and the total energy content of the

wind-generated waves decreased. By the time the long-wave slope was 0·175, the short wind waves had disappeared into the noise level: only the primary long wave with its harmonics is evident.

Two assumptions are necessary if we are to compare these results with the predictions of the theory developed earlier. The first is that, in the absence of mechanically generated waves, the energy density of the wind waves is already limited by small scale breaking. Our photographs and the spectra indicate that this is indeed so at the two longer fetches (7·32 m and 10·36 m), though not at the shortest (4·27 m). Some wave crests were below the height of incipient breaking, some approaching that limit and others that are breaking are presumably subsiding to the point where the small breaking zone can no longer be maintained, when breaking will cease at that particular crest. The second assumption is that the average density in this situation with a narrow spectral range is proportional to (but perhaps rather less than) the energy density in a wave train of the same dominant frequency in which all crests are at the point of incipient breaking. When longer, mechanically generated waves are passing through the wind waves, the latter are limited in the same way at the crests of the long waves, where the drift current is amplified. Again, not every short wave will break on each long-wave crest and the average energy density will vary somewhat with respect to the phase of the long wave as a result of the second-order interactions and the continuing energy input from the wind. Nevertheless, the magnitude of these variations will be small when the long-wave slope is small, so that the average energy density of the wind–wave train will be assumed to be proportional to that in a wave train that is at the point of incipient breaking at the long-wave crest. Accordingly, the ratio of the energy densities in the wind waves with and without mechanically generated waves will be compared with the ratio r^2 calculated from (3.7), where q_0 is the measured value of the surface drift, $q_{\max}$ is found from (3.6) and c_0, the short-wave phase speed at the long-wave crests, from (3.4).

This comparison is shown in figure 7. The continuous curve is calculated for $\alpha = c_0/C = 0{\cdot}5$ and $\gamma = q_0/C = 0{\cdot}196$, corresponding to the measured frequency of the spectral peak and the measured wind drift. The spectra of the wind-generated components at the two larger fetches were integrated numerically over the ranges in which they stand out from the filter shape of the long wave and the energy ratios r^2 were as indicated. The decrease in this ratio is close to, but a little greater than, the reductions predicted by the theory but the agreement is certainly encouraging and lends credence to the idea that the augmentation of the surface drift by the long waves is limiting the energy density of the short waves by decreasing the amplitude at which incipient breaking occurs.

It is worthwhile to examine Mitsuyasu's experiments from the same point of view. These were conducted in a large tank, 70 m long and 8 m wide with a water depth of 2·9 m. A blower with a rectangular orifice was suspended over the tank near the middle, producing a horizontal jet 4 m wide whose axis was approximately 60 cm above the water surface. The air flow of the jet, blowing across the surface, generated waves, but the velocity distribution in the air was not very well defined, being homogeneous neither in the downwind direction nor laterally.

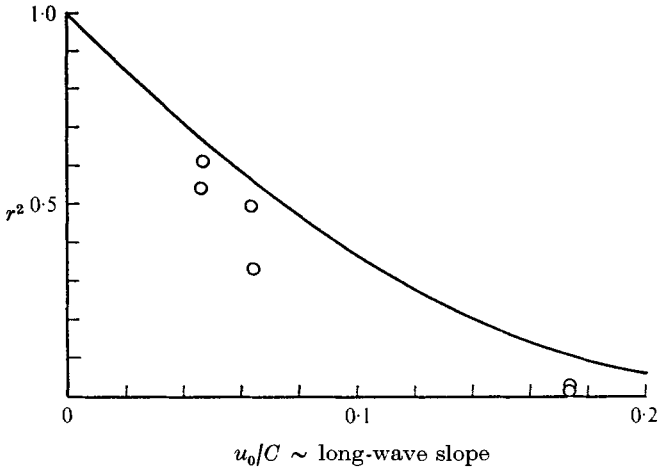

FIGURE 7. The calculated variation in the ratio r^2 of energy density of short waves with and without long waves as a function of u_0/C (long-wave slope, approximately), when $c_0/C = 0{\cdot}5$ and $q_0/C = 0{\cdot}196$. The points are derived by integration of the spectra of figure 6.

Series 1. Peak frequency of wind-generated waves = 2·7 Hz

Mechanically generated wave			Wind wave	
Period T (s)	Height H (cm)	Steepness H/L	'energy' (cm²)	$\frac{c_0}{C}$
—	0	0	1·02	—
1·97	6·5	0·0065	1·03	0·18
1·97	9·2	0·011	0·77	0·18
0·84	5·3	0·040	0·25	0·44

Series 2. Peak frequency of wind-generated waves = 2·6 Hz

—	0	0	1·70	—
1·40	10·3	0·033	0·62	0·27
1·39	8·8	0·022	0·85	0·27
1·38	6·8	0·016	1·07	0·27
1·39	5·5	0·0082	1·36	0·27

TABLE 1. Summary of Mitsuyasu's (1966) results

All measurements were taken at a central location 5·2 m from the nozzle exit; because of the height of the orifice above the surface, the effective fetch was about 4 m. The speed of the jet at the outlet was kept at 20 m/s; 4 m from this point the maximum velocity was approximately 15 m/s. No observations of surface wind drift were reported in Mitsuyasu's (1966) paper but, in correspondence, he estimates $q_0 \sim 42$ cm/s, by extrapolating from measurements with small plastic floats. With the air flow unaltered, Mitsuyasu measured the spectrum of waves generated by the wind alone, and then in the presence of mechanically generated waves produced by a plunger at the end of the tank. Since Mitsuyasu's report

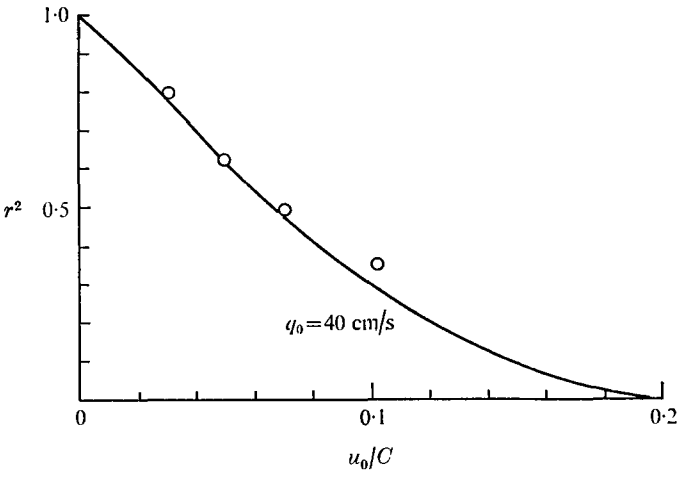

FIGURE 8. The ratio r^2 measured by Mitsuyasu (1966) when $c_0/C = 0{\cdot}27$ for various values of u_0/C.

may not be immediately accessible to readers of this *Journal*, the range of conditions he studied is listed in table 1. Series 2 forms a systematic sequence in which the frequency of the mechanically generated waves is held constant, while the slope progressively increases, a sequence similar to our own described previously. At such a short fetch as this, Mitsuyasu found that the wind–wave spectrum remained peaked about a frequency of 2·6 Hz, with the bulk of the total energy density between 2 and 3 Hz. As the steepness of the mechanically generated wave was increased, again the spectral density and the total 'energy' $\overline{\zeta^2}$ in the wind waves continually decreased.

The measured points derived from Mitsuyasu's data for his series 2 are shown in figure 8, together with the calculated variation of r^2 for $c_0/C = 0{\cdot}27$ as a function of u_0/C, the long-wave slope approximately. The agreement is surprisingly good (better than our own experiments!) but this may be fortuitous. In the series 1 measurements with $c/C = 0{\cdot}18$ and a wave steepness of 0·0065 Mitsuyasu measured an energy ratio of 1·01 (actually an increase) while the calculated value of r^2 with $q_0 = 40$ cm/s is 0·92. With a steepness of 0·011, he measured a ratio of 0·75 while the calculated value is 0·85. The final measurement in series 1 has $c/C = 0{\cdot}44$ and $u_0/C = 0{\cdot}126$; Mitsuyasu measured an energy ratio of 0·24 while, with the same value of q_0, $r^2 = 0{\cdot}20$. Although the comparison between the theory and Mitsuyasu's series 1 measurements is not as striking as that of figure 8, the general consistency between the theory and both his experiments and ours gives confidence that the augmentation of the wind drift at the crests of a train of long waves is indeed limiting the amplitude of short superimposed wind-generated waves.

In the field, with a large fetch, longer waves and swell will provide a local augmentation of the surface wind drift that will similarly reduce the spectral density of the shorter components in the 'saturation range' of the spectrum. But this is something else.

It is a pleasure to acknowledge the gracious and helpful correspondence of Dr Mitsuyasu concerning this work and the support of the Office of Naval Research under Contract N00014-67A-0163-0009.

REFERENCES

BANNER, M. L. 1973 An investigation of the role of short waves and wind drift in the interaction between wind and long gravity waves. Ph.D. dissertation, The Johns Hopkins University.

BANNER, M. L. & PHILLIPS, O. M. 1974 On small scale breaking waves. *J. Fluid Mech.* **65**, 647–657.

BOLE, J. B. & HSU, E. Y. 1967 Response of gravity water waves to wind excitation. *Stanford University Dept. Civil Engng Tech. Rep.* no. 79.

LAMB, H. 1953 *Hydrodynamics.* Cambridge University Press.

LONGUET-HIGGINS, M. S. & STEWART, R. W. 1960 Changes in the form of short gravity waves on long wind waves and tidal currents. *J. Fluid Mech.* **8**, 565–583.

MITSUYASU, H. 1966 Interactions between water waves and wind (I). *Rep. Res. Inst. Appl. Mech., Kyushu University*, **14**, 67–88.

PHILLIPS, O. M. 1968 *The Dynamics of the Upper Ocean.* Cambridge University Press.

WU, J. 1968 Laboratory studies of wind–wave interactions. *J. Fluid Mech.* **34**, 91–111.